

Received December 18, 2020, accepted December 27, 2020, date of publication January 13, 2021, date of current version January 21, 2021.

Digital Object Identifier 10.1109/ACCESS.2021.3051487

Channel Modeling and Over-the-Air Signal Quality at 3.5 GHz for 5G New Radio

ELIJAH I. ADEGOKE¹, ERIK KAMPERT¹, AND MATTHEW D. HIGGINS¹, (Senior Member, IEEE)

WMG, The University of Warwick, Coventry CV4 7AL, U.K.

Corresponding author: Elijah I. Adegoke (elijah.adegoke@warwick.ac.uk)

This work was supported by the Innovate UK via Midlands Future Mobility (MFM) as part of the UK CAM testing facility.

ABSTRACT With the next generation of mobile communication being trialled across the world, 5G New Radio (NR) promises to provide a flexible radio interface that fits a diverse range of use cases. As trials and pilots progress, propagation studies are required that evaluate electromagnetic (EM) propagation effects for 5G NR signals. In this article, 5G NR signals are used to evaluate the over-the-air (OTA) error vector magnitude (EVM) within a line-of-sight (LoS) rural/urban environment. For the same receiver locations, time dispersion and propagation loss were measured via the root mean square (RMS) delay spread and path loss. The transmitter–receiver distance investigated ranged from 60 m to 450 m. From the measurement campaign, the path loss exponent (PLE) using a directional antenna at the receiver was 1.98, and 1.82 with an omnidirectional antenna. The root mean square error (RMSE) of the floating intercept/close-in (FI/CI) models for the path loss was 4.96/4.74 and 3.84/3.23 for directional and omnidirectional receivers. The delay spread using a cross polar configuration showed significant increase and a dependency of the delay spread on the path loss was observed. For the measurement route, the mean delay spread was 24 ns and 35 ns for directional and omnidirectional measurements. With regards to the EVM, 16 and 64-QAM transmissions were robust along the entire route for directional and omnidirectional antennas, whereas 256-QAM worked in locations where there was minimal obstruction to the propagation path. The average EVM (%) for 16, 64 and 256-QAM measured along the route was 4.5/5.3/3.9 and 3.4/4.3/3.6 for omnidirectional and directional antennas. The OTA results also show that using a directional antenna (as the receiver) significantly improves the obtainable signal quality of 5G NR signals and also reduces outages for higher modulation schemes. With the measurement results presented, system designers can design efficient receivers, estimate coverage and adequately provision services using 5G NR on the sub-6 GHz frequency band.

INDEX TERMS Path loss, delay spread, EVM, RF propagation, OTA testing, urban environment, 5G.

I. INTRODUCTION

The 3.5 GHz band presents additional spectrum for 5G services as a complement to already allocated millimeter wave frequency bands. In the UK, this band was recently auctioned to mobile network operators as part of its drive to enable additional capacity for mobile broadband [1], with similar spectrum auctions ongoing around mainland Europe [2]. It is envisaged that this next generation of mobile communications will provide flexible radio access schemes that can support enhanced mobile broadband, ultra-reliable low latency communication as well as massive machine type communications. These components form the pillars of the ITU 5G usage scenarios, some of which include connected

cars, electronic/mobile-health, smart cities and industrial automation [3].

As an opportunistic use case, 5G NR signals can also be used for positioning/localization. The concept of hybrid localization using 5G and satellite signals is being investigated in academia and industry as seen in [4], [5]. Whereas most of the 5G positioning techniques in the literature use time or angle-based ranging [6], it is envisaged that with the adoption of small cells and ultra-dense networks (UDN) [7], [8], 5G received signal strength (RSS)-based ranging will gain increased usage. In RSS based wireless ranging, it is essential that accurate path loss models are used to predict the power–distance relationship [9]. Path loss and fading models such as the free space path loss (FSPL), log-distance model, Hata [10], COST-231 etc. are used to map the received signal power to transmitter–receiver (T–R) distance [9], [11], [12].

The associate editor coordinating the review of this manuscript and approving it for publication was Noor Zaman¹.

In arguably a lot of cases, these models are not representative of most environments [13], [14].

The challenge associated with adequate provisioning and coverage planning of a radio network revolves around accurate modelling of electromagnetic (EM) propagation mechanisms [15]. Large and small-scale fading effects within a specific environment can either be modelled using physics of EM propagation (as in ray tracing), from theoretical methods such as FSPL, or from measurement-based empirical models. Whereas these methods have their respective pros and cons, a combination that is suitable to the design case is usually adopted. From a radio frequency (RF) systems point of view, the case of evaluating the signal quality and performance of an end-to-end (E2E) wireless system is usually done via conducted testing. This creates a gap in controlled laboratory tests and field results/trials, as over-the-air (OTA) effects have not been considered in evaluating the overall performance. As a research contribution to bridge the gap of modelling E2E mobile systems, this article seeks to investigate OTA transmissions of 5G NR signals. By carrying out spot measurements within a line-of-sight (LoS) topography at the University of Warwick campus, path loss, delay spread and OTA error vector magnitude (EVM) were measured. The LoS scenario investigated included partial obstruction from foliage as well as shadow fading from nearby buildings along the path. Given that OTA channel signal quality characterization at 3.5 GHz is extremely limited or non-existent in the literature, this article provides vital information relating to OTA EVM, time dispersion (via RMS delay spread) and radio coverage analysis for outdoor 5G NR communications. Moreover, the measurement environment and scenarios are typical of urban areas. The measurement data from this work can be fed into geometric and statistical models, as well as system-level simulators.

The contributions of this article are summarized as follows:

- 1) Empirical path loss models for directional and omnidirectional receiver configurations are presented in this article. The models obtained are in LoS scenarios within a typical university campus along routes selected for a connected autonomous mobility (CAM) pilot.
- 2) OTA signal quality measurement results are presented in this article for two receiver configurations. The OTA measurements made use of real 5G NR signals to calculate the EVM for modulation schemes used in 5G NR frequency range 1 (FR1).
- 3) Delay spread results are obtained for the same receiver configurations. These results characterize the dispersion in the channel for directional and omnidirectional configurations. The delay spread is an essential parameter in determining how the symbol spacings and lengths in 5G NR signals are affected in real life propagation scenarios.
- 4) In addition to the large and small-scale fading measurements carried out in this work, correlations between the

delay spread and path loss as well as delay spread and OTA EVM are also presented.

The remainder of this paper is organized as follows: Section II presents a concise review of the literature and Section III discusses the background theory of this work. Section IV presents the measurement setup, procedure and the environment in which the measurement campaign was carried out. Section V presents the path-loss model, EVM and delay spread results for directional and omnidirectional scenarios. In Section VI the paper is summarized.

II. RELATED WORK

The measurement campaign carried out in this work can be aligned with propagation measurements at sub-6 GHz frequencies of 5G FR1. In the following section, the related literature is discussed.¹ The academic literature reviewed has been categorized into large-scale and small-scale fading measurements which characterize signal power decay over large wavelengths and signal fluctuations over small wavelengths.

A. LARGE-SCALE FADING MEASUREMENTS

Path loss measurements for 5G 3.4–3.8 GHz ($f_c = 3.5$ GHz) were carried out in [16] for rural, suburban and urban areas around Bern and Zurich in Switzerland. The radio interface of the test bed was based on a time division duplex (TDD) with an OFDM signal occupying a bandwidth of 80 MHz. This setup was capable of 256/64 QAM DL/UL. The measurements were carried out using a base station unit connected via fiber to an active antenna system (AAS) and user equipment (UE) (with eight omnidirectional cross-polarized antennas) as the receiver. The transmit directional antenna gain was 27 dBi and 6 dBi for each element of the receiver antenna. The corresponding transmit beamwidth was 120° azimuth and 30° elevation. To obtain the RSS, the UE was either moved in a van, or pushed by hand to respective measurement locations. At each measurement point, the mobility reference signal power (MRSP) of the dual-polarized beams was recorded. For the measurement route, small-scale fading was averaged out by using a 2-dimensional 5 m grid to bin the measurement points. The LoS/non line-of-sight (NLoS) path loss exponents (PLE) and standard deviation of the shadow fading variable (σ) obtained from their work for the environments investigated were: 2.3/3.1 and 5.1/9.4 dB (rural); 2.9 and 6.9 dB (suburban); 4.8 and 7.1 dB (urban). The authors also compared the channel model parameters obtained for 5G FR1 with a live Long-Term Evolution (LTE) network.

The authors in [17] also characterized the radio channel for 3.5 GHz at the Beijing Jiaotong University, China. The measurement setup was made up of NI software defined radios (SDRs) and an amplifier. The transmitter (T) and receiver (R) were placed at 50 m and 1 m heights. The T–R separation distance investigated in their work was between

¹The 3.5 GHz band was previously used by worldwide interoperability for microwave access (WiMAX) for last mile with cell radius in kilometers. The propagation data presented in this work is steered towards small cells/UDNs with shorter inter-site distance (ISD).

100 m and 250 m. It is envisaged that the authors considered such T–R distances due to the height combination which resembles a mobile radio access network (RAN). In LoS scenarios, the PLE was 6.16 and σ was 4.21 dB. The authors in [18] also carried out path loss measurements in an urban outdoor location around a city hall in Daejeon, Korea for a similar single-input single-output (SISO) system. They used a spread spectrum channel sounder setup with a power amplifier, low noise amplifier (LNA), omnidirectional antennas and a channel analyser module. The transmit power was set to 33 dBm and the T/R heights were 7.3 m/2 m. The PLE and σ obtained from the measurement result over a 500 m T–R distance for NLoS regions was 4.2 and 8.91 dB.

Coverage analysis was carried out using a 5G NR 3.5 GHz test bed in [19]. The radio interface of this measurement setup is similar to [16]. The transmit/reception point (TRP) was made up of an antenna array of 128 cross-polarized antenna elements and the transmit power was set to 40 dBm (5 W). The transmitter was placed at two locations to recreate different radio propagation conditions; with the heights given as 8 m on an outside wall and 20 m on a roof-top. The TRP used also supported digital beamforming with beams spanning $\pm 60^\circ$ (azimuth) and $\pm 15^\circ$ (elevation). By recording the RSS of the mobility reference signals (MRS), coverage and throughput were analysed. The results showed that excess loss was introduced at 3.5 GHz when compared to LTE. This excess loss was compensated for with the beamforming gain. Further path loss measurements at the 5G frequencies of 3.5 GHz and 28 GHz were carried out in [20] for an urban macro-cellular (UMa) scenario. For simultaneous transmission, two individual RF chains (made up of signal generators, power amplifiers and antennas) were used at the transmitter. At the receiver, an ultra-wideband omnidirectional antenna was connected to a spectrum analyser. For T–R distances between 100 m and 200 m, the PLE at 3.5 GHz was 2.15 /2.46 (LoS/NLoS) and 3.26 /6.17 for σ (LoS/NLoS).

Path loss measurements at 3.7 GHz for LoS and NLoS conditions were carried out in [21]. The measurements were taken in Sterea Ellada in Greece for a commercial TD-LTE fixed wireless access (FWA) network. The T–R distances investigated were between 300 m and 1200 m with customer premise equipment (CPEs) used as receiver devices. The CPE antenna system was made up of a 4 x 4 MIMO system and the base station a commercial eNB, placed at 26 m height, with 4 transmit/receive sectorial antennas of 18 dBi gain. The PLE obtained for LoS & NLoS conditions was 2.19 & 2.52 and the slope (β) of the measured path loss curve fit (floating intercept) was 1.73 & 1.87. The standard deviation of the shadowing variable for LoS conditions for both path loss models was 6.0 and 5.8 with corresponding NLoS values as 6.6 and 6.4.

In contrast with the predominant outdoor scenarios described in the above literature, path loss modelling for an indoor-to-outdoor femtocell propagation was investigated in [22]. In the measurement procedure adopted, the path loss

was split into the attenuation from the transmitter to the building facade and attenuation from the facade to the receiver (located on the street). The measurement results showed that the PLE when the transmitter was placed just outside the house followed a power relationship with the frequency and indoor propagation loss varied quadratically with frequency and linearly with the number of walls. At 3.5 GHz, the model obtained generated a RMSE of approximately 10 dB when compared with the measurement data.

Whereas outdoor and indoor radio propagation experience similar EM effects but in varying magnitudes, indoor industrial environments give insightful data as these environments are multipath prone with harsh propagation conditions. In [23], the authors carried out a measurement-based characterization of the channel at 3.5 GHz in industrial and office environments. The measurement setup adopted in this work was an unmodulated 1 MHz baseband signal, with the transmitter placed at 1 m height. The antennas used were omnidirectional with the effective radiated power (ERP) set to 4 dBm. The measurement data showed that in indoor locations, the FSPL resulted in the highest prediction error whereas the multi-wall-floor model provided the least error. Considering all the measurement points, the PLE obtained from the analysis was 3.01. The average shadowing deviation obtained was 7.3 dB when all the locations were considered and 4.35 dB when between two floors in an industrial plant. In addition, the authors also noted that the prediction error using the log-distance model reduced as the shadowing deviation increased.

The authors in [24] also characterised the indoor industrial channel at 3.7 GHz and 28 GHz. The measurements were taken within a high-precision machining workshop with industrial machines and several metallic surfaces. The transmitter and receiver were placed at 1.85 m and 1.44 m height. In a point-to-multipoint topology, the transmitter was fixed with the receiver moved around the machine floor. A time domain channel sounding setup (similar to the method adopted in this article) was adopted, with the transmit power set to 30 dBm and omnidirectional antennas used at both ends of the link. Given that measurements were also taken at 28 GHz, the α /PLE, β , γ and σ of the ABG model fit obtained from the measurements for LoS/NLoS are: 2.27/3.02, 27.29/28.35, 1.94/1.7 and 1.62/1.61.

A summary of the path loss model parameters from the surveyed literature is presented in Table 1.

B. SMALL-SCALE FADING MEASUREMENTS

The measurements in [17] also covered delay spread. From the measurement setup adopted, power delay profiles (PDPs) were obtained at the measurement points by spatial averaging over 20 wavelengths. For the LoS regions investigated in this measurement campaign, the mean delay spread was 45.24 ns. In urban NLoS propagation scenarios, [18] investigated the correlation between path loss, delay spread and K-factor within the Dunsan area, South Korea. The spread spectrum channel sounder was configured for SISO with

TABLE 1. Summary of path loss model parameters of the literature surveyed.

Article	Topography	Environment	Freq.(GHz)	T–R (m)	PLE	β	σ (dB)
[16]	LoS/NLoS	Outdoor	3.5	<2000	2.3/3.1 (rural)		5.1/9.4 (rural)
[17]	LoS	Outdoor	3.5	100–200	6.16		4.21
[18]	NLoS	Outdoor	3.5	<500	4.2		8.91
[19]		Outdoor	3.5				
[20]	LoS/NLoS	Outdoor	3.5	100–200	2.15/2.46		3.26/6.17
[21]	LoS/NLoS	Outdoor	3.7	300–1200	2.19/2.52	1.73/1.87	5.8–6.4
[22]	NLoS	Indoor→outdoor	0.9–3.5				9.99
[23]		Indoor–Machine workshop	3.5	<55	3.01		4.86–13.38
[24]	LoS/NLoS	Indoor–Machine workshop	3.7	≤30	2.27/3.02		1.62/1.61
[26]	LoS/NLoS	Outdoor	3–4	≤120	2/2.7–4.3		4.7–5.1/4.5–7.8

maximum transmit power adopted. Similar to a micro cell, the antenna heights for the transmitter and receiver were 7.3 m and 2 m. With regards to delay spread for the T–R distance (0–500 m), the results showed that the delay spread increased with distance. The maximum/mean delay spread between 300 and 500 m was 4/3 μ s.

A 256 x 16 MIMO setup was used in [25] to obtain propagation characteristics at 3.5 and 6 GHz. The measurement scenario investigated was an urban macro cell (UMa) with the transmitter located on the 7th floor (31 m) and the receiver at 1.8 m. In this measurement campaign, LoS and NLoS propagation cases were investigated with the transmit bandwidth of the channel sounder set to 100 and 200 MHz. Whereas the T–R separation distance is not included, the mean delay spread for both bandwidths in LoS scenarios was 186 and 100 ns. In NLoS scenarios, the corresponding delay spread was 691 and 407 ns, which shows decreasing delay spread with increasing bandwidth. With regards to the accompanying results at 6 GHz, the delay spread also reduced with increasing frequency.

Across the 3–18 GHz band, [26] carried out measurements for path loss and delay spread for UMa and UMi environments. In order to access the wideband channel response in detail, the measurement bandwidth was split into non-overlapping subbands. The measurement setup adopted was based on a real-time frequency-hopping multi-band channel sounder with an arbitrary waveform generator (AWG) capable of generating multitone complex baseband signals. At the receiver, a biconical antenna was connected in tandem to a high pass filter and a LNA. Thereafter, the signals were downconverted and digitized using an analog-to-digital converter (ADC). The measurement environment was a University campus with buildings typical of an urban environment. For UMa scenarios, the transmitter was placed on a rooftop (31 m high) and the receiver on a cart (1.5 m high); for UMi scenarios, the transmitter was placed outside on a wall with varying heights of 8.5 m, 11.5 m and 14 m. In order to average out noise and small-scale fading effects, multiple snapshots were recorded while the receiver moved a set speed on a predefined trajectory. With regards to the measurement results, the subband PLE for 3–4 GHz was close to 2 for UMa LoS and [2.71–4.34] (NLoS). The corresponding mean delay spread was 46 ns (LoS) and 90 ns (NLoS).

At 700 MHz, 2.5 GHz and 3.5 GHz, [27] carried out delay spread measurements around an urban environment in Rio de Janeiro, Brazil. At the transmitter, OFDM signals were transmitted using a signal generator, RF amplifier and sectorial antenna. For reception, an omnidirectional antenna was connected to a LNA and a signal analyser. With the transmitter placed on a rooftop and the receiver in a car, the environment can be likened to a UMa cell. While the results do not explicitly classify LoS from NLoS, the mean delay spread at 3.5 GHz was 49 ns and was observed to decrease as frequency increases.

Delay spread measurements were also carried out in [24] to accompany the path loss measurements. At 3.7 GHz, the mean delay spread was 20.3 ns and 37.4 ns for LoS and NLoS receiver locations. From the corresponding delay spread CDF, 90% of the RMS delay spread was lower than 27 ns and 45 ns for LoS and NLoS. In a smaller machine workshop with similar inventory at a University, delay spread measurements were carried out at 3.5 GHz in [28] using a frequency domain method. In this work, both the transmitter and receiver were at the same height of 1.5 m with the same omnidirectional antenna used at both ends of the link. For LoS and NLoS receiver points, the mean delay spread was 15.77 ns and 24.37 ns. The delay spread for LoS and NLoS was less than 18 ns and 27 ns for 90% of the delay spread CDF. Also included in this work are Saleh-Valenzuela parameters obtained from a virtual array. Intuitively, the values reported in this work are lower than the results presented in [24] as the University workshop has a smaller footprint and inventory.²

In Table 2, a summary of the RMS delay spread parameters from the surveyed literature is presented.

III. EMPIRICAL PATH LOSS MODELLING

For a transmitter and a receiving device, the power received decays as the T–R separation distance increases. The RSS can be obtained analytically using the free space path loss equation

$$L_{\text{FSPL}} = 20 \log_{10} \left(\frac{4\pi d}{\lambda} \right) \quad (\text{dB}) \quad (1)$$

²For an extensive survey on 5G channel measurements and modelling, readers are directed to [29].

TABLE 2. Summary of RMS delay spread parameters of the literature surveyed.

Article	Topography	Environment	Freq.(GHz)	T–R (m)	Mean delay (ns)
[17]	LoS	Outdoor	3.5	100–250	45.24
[18]	NLoS	Outdoor	3.5	300–500	3000
[25]	LoS/NLoS	Outdoor	3.5		100/407 (200 MHz)
[26]	LoS/NLoS	Outdoor	3–4	≤120	46/90
[27]	LoS/NLoS	Outdoor	3.5		49
[24]	LoS/NLoS	Indoor–Machine workshop	3.7	≤30	20.30/37.40
[28]	LoS/NLoS	Indoor–Machine workshop	3.5	<15	15.77/24.37

where d is the T–R separation distance, and λ is the wavelength. However, in order to obtain realistic link budgets, a common approach is to adopt a combination of both theoretical and empirical models [12]. With respect to measurement-based coverage models, the log-normal shadowing model in (2) is widely adopted for modelling path loss and T–R separation distance,

$$PL = A + 10n \log_{10} \left(\frac{d}{d_o} \right) + X_{\sigma} \quad (dB) \quad (2)$$

where X_{σ} is a Gaussian random variable with zero mean and variance (σ^2), d_o is the reference distance (m), and n is the PLE. The shadowing variable X_{σ} can be obtained by carrying out linear regression on the measurement and predicted data using (3)

$$\sigma = \sqrt{\sum_{i=1}^N \frac{(P_{meas}(i) - P_{pred})^2}{N - 1}} \quad (dB) \quad (3)$$

where $P_{meas}(i)$ is the i^{th} measured path loss, P_{pred} is the mean predicted path loss and N is the total number of samples.

Apart from the generic log-distance model in (2), empirical models from different measurement campaigns as well as standard organisations and research groups are available in the literature. With regards to these models, they are typically oriented towards the floating intercept (FI) as seen in WINNER-II and 3GPP or close-in (CI) path loss modelling. A FI path loss model can be represented as:

$$PL = \alpha + 10\beta \log_{10}(d) + X_{\sigma} \quad (dB) \quad (4)$$

where α is the y -intercept, and β is the slope of the regression line. The model presented in (2) is regarded as CI when A is calculated as the free space path loss at reference distance (d_o). The value of A at d_o can either be obtained from averaging path loss measurements at d_o or from (1) with the antenna gains included. For CI path loss models, A remains constant for $d > d_o$ [30]–[32].

IV. MEASUREMENT ENVIRONMENT, SETUP AND PROCEDURE

The measurements presented in this paper were taken at the University of Warwick's main campus. The transmitter was placed on the terrace of the Lord Bhattacharyya building (LBB), with staggered measurements taken from the LBB towards the University Nursery. The view from the transmitter towards the receiver is shown in Fig. 1. The environment



FIGURE 1. View from the transmitting antenna on the Professor Lord Bhattacharyya Building, for the measurements of a sample urban environment (part of Midlands Future Mobility) approximately 400 m in length with a variety of common structures, objects and construction materials.

selected can be classified as LoS given that there is a clear path from the roof top of the LBB towards the Nursery. There is sparse foliage along the path with low height buildings located on either side of the road. The average road width is 5 m. The route selected is part of the University's proposed autonomous transport service route. It is envisaged that this route will be used to offer a connected automated mobility (CAM) service.

The setup adopted in this work is based on R&S channel sounding and 5G equipment. For path loss and delay spread, a time domain channel sounding technique was used. The channel sounding equipment uses the pulse compression method and consists of a R&S SMBV100B Vector Signal Generator (VSG), a R&S BBA150 Broadband Amplifier, two R&S TSMX-PPS2 GPS modules, and a R&S FSV3007 Signal and Spectrum Analyzer. The former two devices enable the transmission of frequency band limited signals up to 6 GHz and an arbitrary modulated waveform with clock frequencies up to 300 MHz. The latter device enables the processing of the received signals with a maximum sampling rate of 400 MHz. The resulting I/Q data are forwarded to the R&S Channel Sounding Software, which autocorrelates the received I/Q data with the originally transmitted signal. The equipment is time-synchronized by means of GPS signals, with a typical RMS jitter of 30 ns. A 300 MHz bandwidth signal was generated and analyzed, providing a

TABLE 3. Link budget and Setup Specifications for Channel Sounding.

Parameter	Symbol	Value (unit)
Directional antenna gain	G_d	11 dBi
Amplifier (Amp) gain	G_{amp}	+10
RF power supplied to antenna	P_{tG}	+35.7 dBm
Omnidirectional antenna gain	G_o	3 dBi
Long cable loss	L_c	8 dB
Max. measurable path loss		120 dB

time resolution of 3.3 ns, equivalent to a spatial resolution of 1 m. A filtered Frank-Zadoff-Chu sequence [33] with a length of 120,000 samples was used as a channel sounding waveform, resulting in a channel impulse response (CIR) update rate of 400 μ s. Per antenna constellation, 512 CIR measurements were automatically triggered, and their results were stored, averaged and further analyzed.

For EVM measurements, the VSG was configured to 5G NR (R15) downlink specifications. For 16-, 64- and 256-QAM, the bandwidth parts (BWPs) in a single cell were modified using the flexible numerology available in the device. Guided by the reference channel information in TS 38.101-1 [34], EVM measurements were carried out for three M -ary modulation schemes using 30 and 60 kHz subcarrier spacing (SCS) and channel bandwidth of 100 MHz. The cell deployment option was 3 GHz $< f \leq$ 6 GHz with a Case B synchronisation signal (SS/PBCH). The SS/PBCH blocks use a SCS of 30 kHz and the BWPs use SCS of 30 kHz and 60 kHz. Three nonoverlapping BWPs were used with the physical downlink shared channel (PDSCH) on each BWP configured for different modulation schemes. Similar resource blocks were allocated to the BWPs, such that the channel bandwidth was split evenly. In order to demodulate the 5G signal, the configurations and signal descriptions are replicated in the spectrum analyser. In addition, phase compensation at 1 GHz was included in the signal generator and spectrum analyser.

The link budget of the setup is presented in Table 3. With respect to path loss modelling in this paper, the propagation loss experienced from transmitter to receiver is expressed as:

$$PL(d) = P_{tG} + G_t + G_r - P_r - 2L_c \quad (dB) \quad (5)$$

where P_{tG} is the amplified power fed to the transmitting antenna via a long RF cable ($P_t + G_{amp} - L_c$) in dBm, G_t is the directional gain of the transmitter in dBi, G_{amp} is the gain of the high power amplifier, L_c is cable loss and P_r is the received power in dBm. The receiver antenna gain can be represented as G_r in dBi when an omnidirectional antenna is used and $G_r(\phi, \theta)$ for a directional antenna. For the channel sounder, the maximum propagation loss that can be measured is approximately 120 dB. Exceeding this propagation loss, the multipath components (MPC) in the PDP are not distinct as the signal becomes buried within the noise floor. In order to reduce the effect of body/vehicle shadowing, the measurements were mostly carried out at off-peak times or during other periods with minimal vehicle and human traffic.

V. MEASUREMENT RESULTS AND ANALYSIS

The measurement results are discussed in three parts. The first part presents propagation loss results, the second addresses time dispersion in the wireless channel using the same setup, and in the third part, EVM from 5G NR compliant (R15) devices are used to evaluate the OTA signal quality.

A. PATH LOSS AND COVERAGE PLANNING

In Figs. 2 and 3, the curve fit/FI and CI model obtained from the measurement data is presented for directional and omnidirectional measurements. For the CI model fit (PLE, σ), parameter A was obtained from measurements and the PLE was obtained by performing a minimum mean square error (MMSE) regression to the received power. The parameters of the FI model (α, β, σ) were obtained by performing a least squares regression to the measured path loss. The empirical models and parameters obtained from the measurement campaign are presented in Tables 4 & 5 and the corresponding error statistics in Table 6. The RMSE and parameters of the FI and CI models show that the empirical models can be regarded as representative of the environment, as the cumulative prediction error is minimal. In Figs. 2 and 3, the propagation loss experienced increases from 150 m to 190 m. This is because the pedestrian path on which the receiver was placed bends away from the transmitter, upon approaching the roundabout. Thus, the receiver drifts into an obstructed LoS resulting from foliage. In addition to this, the receiver is not aligned with the transmitter anymore. With regards to the trend of the power decay as the receiver approaches the roundabout, a model fit for the first half of the route for the omnidirectional receiver is shown in Fig. 4. At approximately 250 m, where the measurement resumes at the other side of the roundabout, the foot path aligns with the transmit antenna boresight. This causes the path loss to initially drop.³ A prolonged deep fade is then experienced along the path due to buildings on either side of road. At the end of the route, the foot path bends and causes the path loss to increase as the receiver drifts into an obstructed LoS. The prolonged shadow fading resulting from the environment along this path is also shown in the delay spread and OTA EVM results.

The PLE from Table 5 shows that a typical PLE of 2 for both directional and omnidirectional antenna measurement can be adopted for the environment investigated. In comparison with the academic literature discussed in Section III, the PLE obtained can be aligned with measurement campaigns in similar environments. With respect to the type of model, the CI model requires less parameters and can be easily adopted as the reference path loss can be readily computed or estimated. Moreover, from this particular measurement campaign, the standard deviation (σ) of the shadow variable from both models are approximately equal.

³Given the T–R distances investigated in this work, it is envisaged that different model parameters will be required for distances beyond the “breakpoint”. The breakpoint is defined for distances where the first fresnel zone gets blocked by the ground.

TABLE 4. Floating Intercept Path Loss Model (α, β, σ).

Environment	Description	Model	α	β	σ [dB]
LoS (Direc – Direc)	Combined Path	$37 + 19.2 \log_{10}d$	37.04	1.92	6.89
LoS (Direc – Direc)	[60 190]	$-20.55 + 47.60 \log_{10}d$	-20.55	4.76	7.75
LoS (Direc – Direc)	[255 440]	$-18.13 + 40.50 \log_{10}d$	-18.13	4.05	4.97
LoS (Direc – Omni)	Combined Path	$51 + 12.7 \log_{10}d$	50.51	1.27	4.87
LoS (Direc – Omni)	[60 190]	$-2.45 + 39.90 \log_{10}d$	-2.45	3.99	5.89
LoS (Direc – Omni)	[255 440]	$24.28 + 23.50 \log_{10}d$	24.28	2.35	3.48

TABLE 5. Close-in Path Loss Model (PLE, σ).

Environment	Description	Model	PLE	σ [dB]
LoS (Direc – Direc)	Combined Path	$35.73 + 19.8 \log_{10}d/d_o$	1.98	6.89
LoS (Direc – Direc)	[60 190]	$35.73 + 20.70 \log_{10}d/d_o$	2.07	7.73
LoS (Direc – Direc)	[255 440]	$35.73 + 19.40 \log_{10}d/d_o$	1.94	4.99
LoS (Direc – Omni)	Combined Path	$39.26 + 20.7 \log_{10}d/d_o$	1.82	4.89
LoS (Direc – Omni)	[60 190]	$39.26 + 19.90 \log_{10}d/d_o$	1.99	5.91
LoS (Direc – Omni)	[255 440]	$39.26 + 17.60 \log_{10}d/d_o$	1.76	3.50

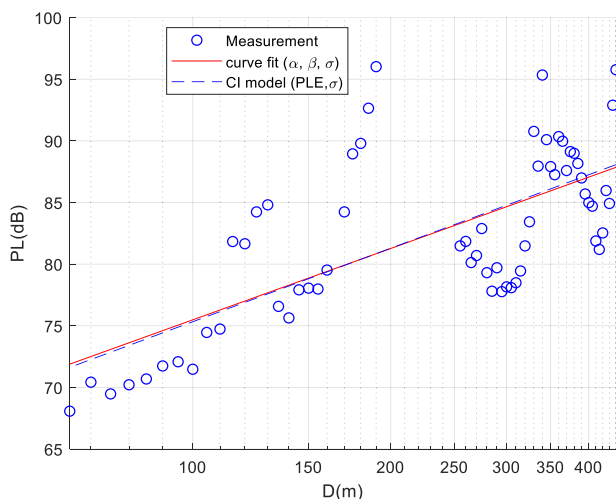


FIGURE 2. LoS Path loss models for directional measurement data. CI reference distance ($d_0 = 1$ m) and A obtained from measurements.

TABLE 6. RMSE for empirical path loss models (Combined path).

Environment	Model	RMSE (dB)
Direc – Direc	FI	4.96
	CI	4.74
Direc – Omni	FI	3.84
	CI	3.23

For the CI model, the choice of the reference distance has an effect on the PLE, thus it is essential to adopt a reference distance that is close to the transmit antenna. Associating the slope of the FI model (β) with the PLE has been contested in the literature [21], [30], [35] and while addressing the comparison is outside the scope of this article, the slope (β) of the path loss regression lines is between 1.3 and 2 for omnidirectional and directional.

While the T–R distances presented in this work are less than 1 km, coverage planning will require properly calculated link budgets. The shadow fading variable gives communication system planners some flexibility in estimating the path loss from empirical models, as it is expected that in most cases

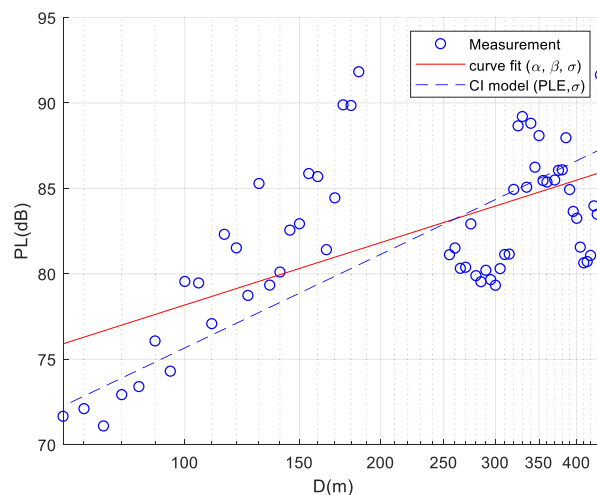


FIGURE 3. LoS Path loss models for omnidirectional measurement data. CI reference distance ($d_0 = 1$ m) and A obtained from measurements.

these parameters will vary from one environment to another. In this regard, adopting suitable probability distributions that describe the shadow variable can improve coverage planning when adopting empirical models.

B. DELAY SPREAD

The time dispersion in the wireless channel can be characterised using the RMS delay spread, excess delay, or excess delay spread. These parameters allow comparison of multipath channels for wireless system designs [12]. In the academic literature, the RMS delay spread is mostly used. Using the channel sounding measurement setup described in Section IV, the delay spread at each point was obtained from the average power delay profile (APDP) at each measurement point. In Fig. 5, the APDPs for directional and omnidirectional from one of the measurement points (at $d = 300$ m) is shown. The delay spread at each measurement point can be obtained from

$$\tau_{rms} = \sqrt{\frac{\int_0^\infty (\tau - \bar{\tau})^2 \cdot APDP(\tau) d\tau}{\int_0^\infty APDP(\tau) d\tau}} \quad (6)$$

where $\bar{\tau}$ is the mean delay given by

$$\bar{\tau} = \frac{\int_0^\infty \tau \cdot \text{APDP}(\tau) d\tau}{\int_0^\infty \text{APDP}(\tau) d\tau} \quad (7)$$

The CDF of the delay spread from the measurement campaign is shown in Fig. 6. In Fig. 7, the delay spread is plotted against T–R separation distance. From the CDF and the delay spread versus distance, it can be seen that the *Dirac–Dirac* setup significantly reduces the dispersion in the channel. For measurements with the omnidirectional receiver, the delay spread gradually increases with distance, whereas the measurements from the directional antenna are bounded. Closer to the transmitter, foliage causes the delay spread to increase as the receiver moves further away. From the CDF figures, 90% of the RMS delay spread is less than 40 ns, 60 ns and 95 ns for the directional, omnidirectional and cross polar omnidirectional receiver configurations. Intuitively, the cross polar measurements show an increased delay spread due to polarization mismatch. The mean delay spread for the three receiver/environment combination are 24 ns, 36 ns and 57 ns. In Table 7, a comparison is presented that summarises the RMS delay spread. This table reiterates the fact that the time dispersion in the channel can be minimized using directional antennas. The standard deviation also shows that using a directional antenna bounds the delay spread. Furthermore, for measurements using the directional antenna at the receiver, most of the received power is in the LoS MPC. In comparison with the delay spread values presented in Section III, the values obtained from this measurement campaign are similar as they are of the same order.

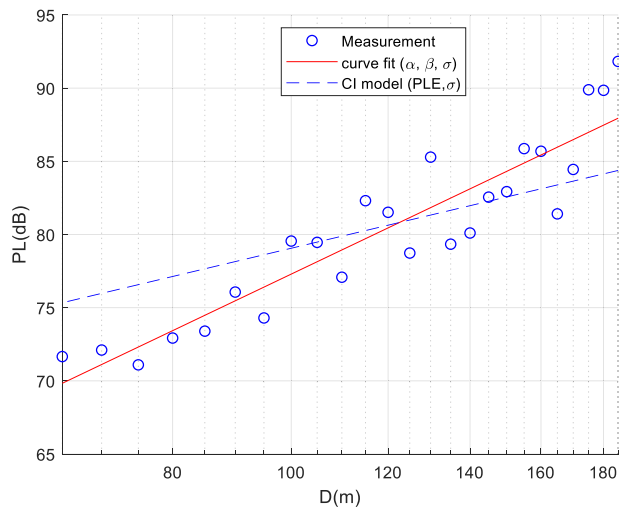


FIGURE 4. LoS Path loss models for omnidirectional measurement data for 60 – 100 m. CI reference distance ($d_0 = 1$ m) and A obtained from measurements.

As seen in the path loss measurements, a prolonged deep fade can be noticed along the route from 320 to 370 m. The authors explain this to be due to shadow fading resulting from the combination of various types of university

TABLE 7. Mean, standard deviation, minimum and maximum RMS delay spread.

Environment	μ (ns)	σ (ns)	Min. (ns)	Max. (ns)
Dirac – Dirac	24.5	11.5	12.4	68.9
Dirac – Omni	35.5	14.8	19.1	83.6
Xpolar–Omni	57.1	23.0	29.2	123.3

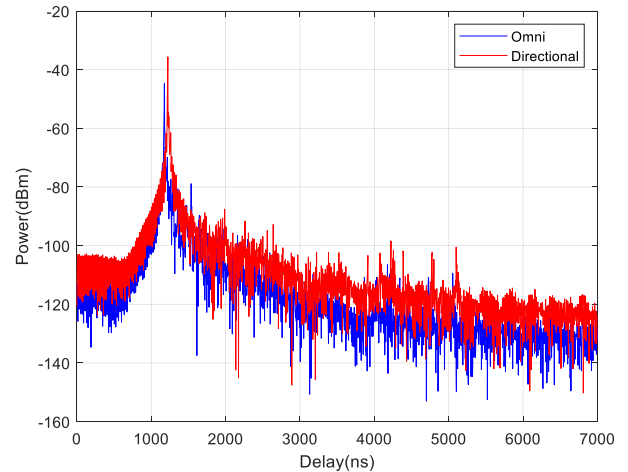


FIGURE 5. Average power delay profile for directional and omnidirectional measurements ($d = 300$ m).

buildings close to the receiver along the route. While the cross polarisation measurements show no indication of depolarisation, prolonged deep fades in some environments can be associated with this effect [36]. In cases where depolarisation is prevalent, techniques such as polarization diversity, rotating polarization [37] or polarization hopping [36] can be adopted in the transmitter or receiver RF system design.

The relationship between delay spread and path loss was also investigated. In Fig. 8, a plot of the path loss versus RMS delay spread is presented. From the plot, it can be seen that there is a correlation between path loss and delay spread for both antenna types. The correlation is lower for omnidirectional measurements with R^2 lower than 0.5. A stronger correlation exists for the directional measurements with $R^2 = 0.77$. The results generally show that as the path loss increases, the delay spread also increases which aligns with the literature [38].

TABLE 8. EVM PDSCH Limits from 3GPP TS 38.101-1 [34].

PDSCH Modulation	Limit (%)
QPSK	18.50
16-QAM	13.50
64-QAM	9.00
256-QAM	4.50

C. OTA EVM

For each constellation in the 5G NR signal, the EVM limits for the three M-ary modulation schemes used are presented in Table 8. At the same measurement locations used for channel sounding, the OTA EVM was measured using a

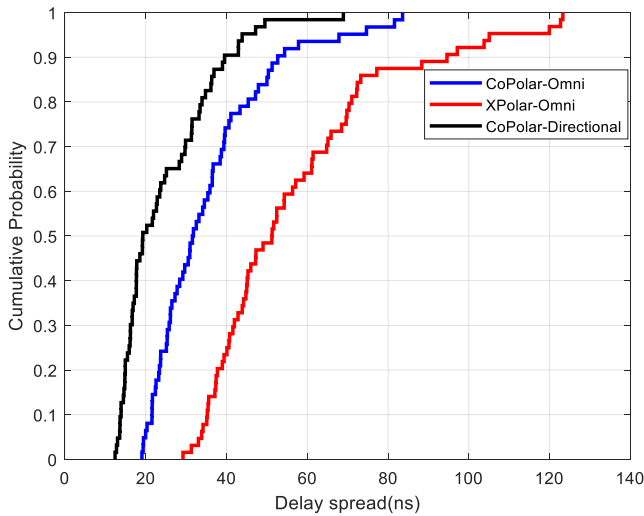


FIGURE 6. Delay spread CDF for omnidirectional (co & cross-polar) and directional measurements.

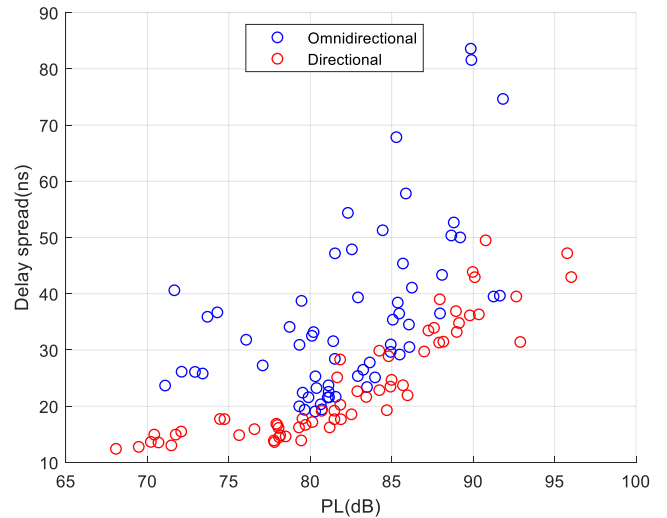


FIGURE 8. Path loss versus delay spread for omnidirectional and directional measurements.

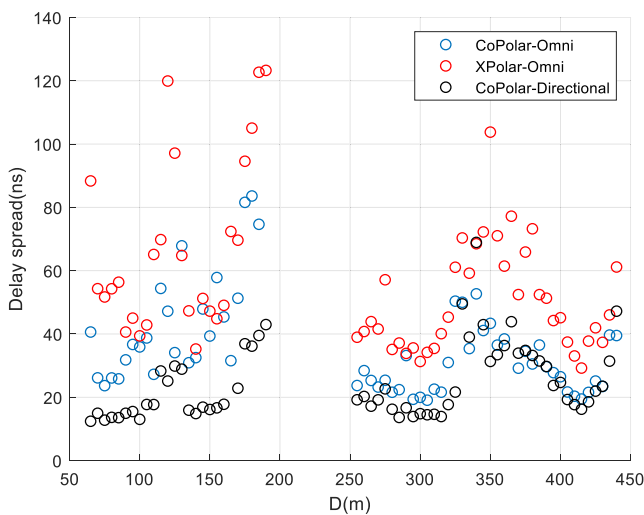


FIGURE 7. Delay spread versus distance for directional and omnidirectional measurements.

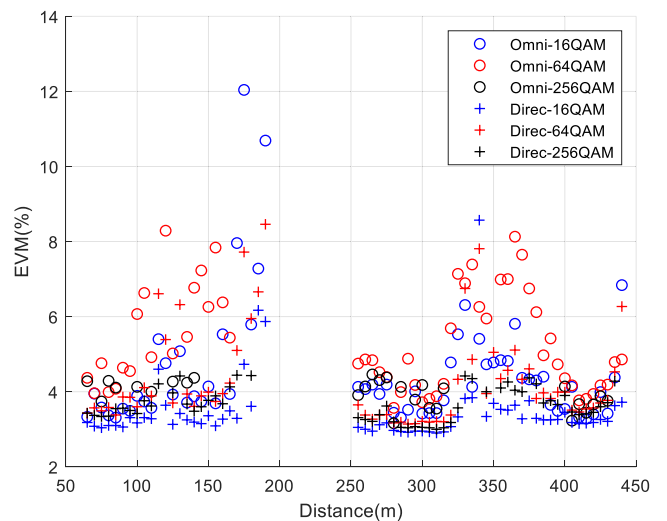


FIGURE 9. OTA EVM for directional and omnidirectional measurements.

directional and omnidirectional antenna. The OTA EVM can be adopted as an alternative to bit error rate (BER), as it can be used to estimate the performance of a wireless link without a complete protocol stack. The OTA EVM and distance relationship for the measurement route is shown in Fig 9. Visually observing the OTA EVM results, it can be seen that the EVM using a directional antenna at the receiver is generally below 4% at most measurement points. While improved signal quality is available using a directional antenna at the receiver, occasionally this requires that the receiver is visually aligned with the transmitter. As a result, this might not be a feasible use case as the location of the transmitters in most cases is not known a priori. Nonetheless, with smart antenna technologies such as beam steering, an improved link quality can be obtained at the expense of additional signal processing. With regards to the prolonged deep fade highlighted in the channel sounding results (in Figs. 2, 3 and 7)), a similar same trend

is evident in Fig. 9. This also indicates that while slightly different setups and configurations are used, the results are consistent with each other.

The OTA EVM for the 5G NR signals has also been compared with the channel sounding results at the same measurement locations. With respect to the interdependencies between delay spread and OTA EVM, an increasing trend can be observed as shown in Fig. 10. From Fig. 10, it is evident that for enhanced quality of service (QoS), the time dispersion in the channel needs to be less than 30 ns. This is because with lower delay spread, the corresponding EVM (%) is lower than the upper limit and the receiver is able to use higher order modulation schemes across the channel. Combining this with the path loss— delay spread results and the provided link budget, the corresponding path loss also needs to be less than 80 dB for omnidirectional and 87.5 dB for directional. This alongside the results shown in Fig. 8 shows that the OTA signal quality, path loss and the time dispersion in the channel

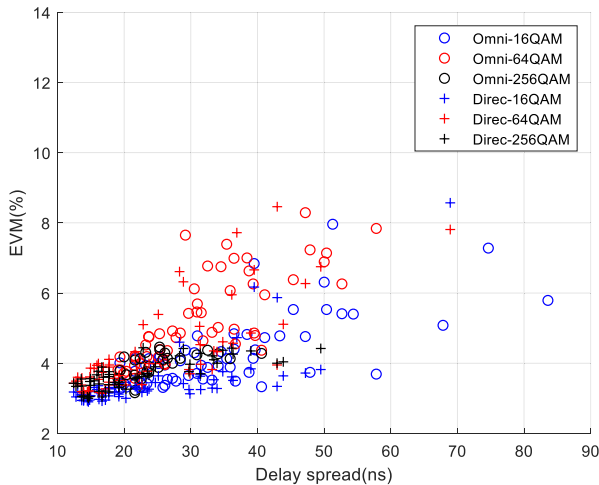


FIGURE 10. OTA EVM and delay spread for the M-ary 5G NR waveform.

are closely related and can be used to characterise the wireless channel as well as the QoS.

VI. CONCLUSION

This paper has presented the first OTA EVM measurements at the sub-6 GHz 5G band using 5G NR signals in a point-to-multipoint scenario. The measurement campaign covers large and small-scale fading effects that are reported via the path loss and delay spread. The channel quality has also been investigated using 5G NR signals configured with a flexible radio interface in terms of the OTA EVM. Two antenna types have been investigated in this work, the directional antenna improves the signal quality, and reduces outages for higher modulation schemes as well as time dispersion in the channel. The directional and omnidirectional PLEs from the measurement campaign are 1.98 and 1.82 for a LoS environment. The dependencies between delay spread and path loss as well as EVM were also presented. The results show that an increased path loss is linked with an increased delay spread, and that EVM is proportional to delay spread. The mean RMS delay spread using a directional and omnidirectional antenna was 24 ns and 35 ns, which shows that the environment is suitable for multiple antenna communications. The effect of cross polarization was also investigated with regards to delay spread. Intuitively, this cross-polar setup causes the delay spread to increase using an omnidirectional receiver whereas the signal is entirely lost for the directional antenna used. Using a directional antenna at the receiver results in better communications conditions, however, factors relating to steering or switching of the beam are required for beam alignment with the transmitter. The measurement results presented in this work can be adopted in channel models and OTA testing methods for 5G NR communication systems. As future work, measurements in the LoS scenario presented in this article will be carried out for millimeter wave frequencies as well as performance evaluation of the sub 6 GHz empirical models in similar environments around the University campus.

REFERENCES

- [1] Ofcom. *Award of 2.3 and 3.4 GHz Spectrum by Auction*. Accessed: Feb. 5, 2020. [Online]. Available: <https://www.ofcom.org.uk/spectrum/spectrum-management/spectrum-awards/awards-archive/2-3-and-3-4-ghz-auction>
- [2] T. Leins. *A Guide to 5G Spectrum Auctions in Western Europe: From Austria to France to The Netherlands*. Accessed: Feb. 5, 2020. [Online]. Available: <https://blog.telegeography.com/a-guide-to-5g-spectrum-auctions-in-western-europe-austria-france-germany-netherlands-switzerland>
- [3] ITU-T Telecommunication Standardization. *Emerging Trends in 5G/IMT2020*. Accessed: Feb. 5, 2020. [Online]. Available: <https://www.itu.int/en/membership/Documents/missions/GVA-mission-briefing-5G-28Sept2016.pdf>
- [4] G. Destino, J. Saloranta, G. Seco-Granados, and H. Wymeersch, "Performance analysis of hybrid 5G-GNSS localization," in *Proc. 52nd Asilomar Conf. Signals, Syst., Comput.*, Oct. 2018, pp. 8–12.
- [5] J. A. del Peral-Rosado, D. Bartlett, F. Grec, L. Ries, R. Prieto-Cerdeira, J. A. Lopez-Salcedo, G. Seco-Granados, O. Renaudin, C. Gentner, R. Rauliefs, E. Dominguez-Tijero, A. Fernandez-Cabezas, F. Blazquez-Luengo, G. Cueto-Felgueroso, and A. Chassaingne, "Physical-layer abstraction for hybrid GNSS and 5G positioning evaluations," in *Proc. IEEE 90th Veh. Technol. Conf. (VTC-Fall)*, Sep. 2019, pp. 1–6.
- [6] H. Wymeersch, N. Garcia, H. Kim, T. Walter, G. Seco-Granados, S. Kim, and F. Wen, "5G mm wave downlink vehicular positioning," in *Proc. IEEE Global Commun. Conf.*, Dec. 2018, pp. 206–212.
- [7] V. Jungnickel, K. Manolakis, W. Zirwas, B. Panzner, V. Braun, M. Lossow, M. Sternad, R. Apelfrojd, and T. Svensson, "The role of small cells, coordinated multipoint, and massive MIMO in 5G," *IEEE Commun. Mag.*, vol. 52, no. 5, pp. 44–51, May 2014.
- [8] J. Werner, M. Costa, A. Hakkarainen, K. Leppanen, and M. Valkama, "Joint user node positioning and clock offset estimation in 5G ultra-dense networks," in *Proc. IEEE Global Commun. Conf. (GLOBECOM)*, Dec. 2014, pp. 1–7.
- [9] A. Bel, J. L. Vicario, and G. Seco-Granados, "Localization algorithm with on-line path loss estimation and node selection," *Sensors*, vol. 11, no. 7, pp. 6905–6925, Jul. 2011. [Online]. Available: <http://www.mdpi.com/1424-8220/11/7/6905>
- [10] M. Hata, "Empirical formula for propagation loss in land mobile radio services," *IEEE Trans. Veh. Technol.*, vol. 29, no. 3, pp. 317–325, Aug. 1980.
- [11] C. C. Pu, B. G. Lee, W.-Y. Chung, and P. C. Ooi, "Analysis of path loss exponent error in ranging and localization of wireless sensor network," in *Proc. Int. Conf. Frontiers Commun., Netw. Appl. (ICFCNA-Malaysia)*, 2014, pp. 1–6.
- [12] T. Rappaport, *Wireless Communications: Principles and Practice*, 2nd ed. Upper Saddle River, NJ, USA: Prentice-Hall, 2001.
- [13] T. O. Olasupo, C. E. Otero, L. D. Otero, K. O. Olasupo, and I. Kostanic, "Path loss models for low-power, low-data rate sensor nodes for smart car parking systems," *IEEE Trans. Intell. Transp. Syst.*, vol. 19, no. 6, pp. 1774–1783, Jun. 2018.
- [14] X. Li, "RSS-based location estimation with unknown pathloss model," *IEEE Trans. Wireless Commun.*, vol. 5, no. 12, pp. 3626–3633, Dec. 2006.
- [15] E. I. Adegoke, E. Kampert, and M. D. Higgins, "Empirical indoor path loss models at 3.5 GHz for 5G communications network planning," in *Proc. Int. Conf. UK-China Emerg. Technol. (UCET)*, Aug. 2020, pp. 1–4.
- [16] A. Schumacher, R. Merz, and A. Burg, "3.5 GHz coverage assessment with a 5G testbed," in *Proc. IEEE 89th Veh. Technol. Conf. (VTC-Spring)*, Apr. 2019, pp. 1–6.
- [17] R. He, M. Yang, L. Xiong, H. Dong, K. Guan, D. He, B. Zhang, D. Fei, B. Ai, Z. Zhong, Z. Zhao, D. Miao, and H. Guan, "Channel measurements and modeling for 5G communication systems at 3.5 GHz band," in *Proc. URSI Asia-Pacific Radio Sci. Conf. (URSI AP-RASC)*, Aug. 2016, pp. 1855–1858.
- [18] B.-G. Yeo, B. J. Lee, and K.-S. Kim, "Channel measurement and characteristics analysis on 3.5 GHz outdoor environment," in *Proc. 1st Int. Conf. Green Commun., Comput. Technol. (GREEN)*, Jul. 2016, pp. 11–14.
- [19] B. Halvarsson, A. Simonsson, A. Elgcróna, R. Chana, P. Machado, and H. Asplund, "5G NR testbed 3.5 GHz coverage results," in *Proc. IEEE 87th Veh. Technol. Conf. (VTC Spring)*, Jun. 2018, pp. 1–5.
- [20] K. Zhang, R. Zhang, J. Wu, Y. Jiang, and X. Tang, "Measurement and modeling of path loss and channel capacity analysis for 5G UMa scenario," in *Proc. 11th Int. Conf. Wireless Commun. Signal Process. (WCSP)*, Oct. 2019, pp. 1–5.

- [21] N. Moraitis, D. Vouyioukas, A. Gkioni, and S. Louvros, "Measurements and path loss models for a TD-LTE network at 3.7 GHz in rural areas," *Wireless Netw.*, vol. 26, no. 4, pp. 1572–8196, 2020.
- [22] A. Valcarce and J. Zhang, "Empirical indoor-to-outdoor propagation model for residential areas at 0.9–3.5 GHz," *IEEE Antennas Wireless Propag. Lett.*, vol. 9, pp. 682–685, 2010.
- [23] T. Chrysikos, P. Georgakopoulos, I. Oikonomou, and S. Kotsopoulos, "Measurement-based characterization of the 3.5 GHz channel for 5G-enabled IoT at complex industrial and office topologies," in *Proc. Wireless Telecommun. Symp. (WTS)*, Apr. 2018, pp. 1–9.
- [24] M. Schmieder, T. Eichler, S. Wittig, M. Peter, and W. Keusgen, "Measurement and characterization of an indoor industrial environment at 3.7 and 28 GHz," in *Proc. 14th Eur. Conf. Antennas Propag. (EuCAP)*, Mar. 2020, pp. 1–5.
- [25] Z. Zheng, J. Zhang, Y. Yu, L. Tian, and Y. Wu, "Propagation characteristics of massive MIMO measurements in a UMa scenario at 3.5 & 6 GHz with 100 & 200 MHz bandwidth," in *Proc. IEEE 28th Annu. Int. Symp. Pers., Indoor, Mobile Radio Commun. (PIMRC)*, Oct. 2017, pp. 1–5.
- [26] V. Kristem, C. U. Bas, R. Wang, and A. F. Molisch, "Outdoor wideband channel measurements and modeling in the 3–18 GHz band," *IEEE Trans. Wireless Commun.*, vol. 17, no. 7, pp. 4620–4633, Jul. 2018.
- [27] M. M. Silva, L. da Silva Mello, C. V. Rodriguez, M. P. C. Almeida, and P. G. Castellanos, "Urban mobile channel delay spread measurements at 700 MHz, 2.5 GHz and 3.5 GHz," in *Proc. 12th Eur. Conf. Antennas Propag. (EuCAP)*, 2018, pp. 1–4.
- [28] E. I. Adegoke, R. M. Edwards, W. G. Whittow, and A. Bindel, "Characterizing the indoor industrial channel at 3.5 GHz for 5G," in *Proc. Wireless Days (WD)*, 2019, pp. 1–4.
- [29] C.-X. Wang, J. Bian, J. Sun, W. Zhang, and M. Zhang, "A survey of 5G channel measurements and models," *IEEE Commun. Surveys Tuts.*, vol. 20, no. 4, pp. 3142–3168, 4th Quart., 2018.
- [30] T. S. Rappaport, G. R. MacCartney, M. K. Samimi, and S. Sun, "Wideband millimeter-wave propagation measurements and channel models for future wireless communication system design," *IEEE Trans. Commun.*, vol. 63, no. 9, pp. 3029–3056, Sep. 2015.
- [31] G. R. MacCartney and T. S. Rappaport, "Rural macrocell path loss models for millimeter wave wireless communications," *IEEE J. Sel. Areas Commun.*, vol. 35, no. 7, pp. 1663–1677, Jul. 2017.
- [32] A. F. Molisch, L. J. Greenstein, and M. Shafi, "Propagation issues for cognitive radio," *Proc. IEEE*, vol. 97, no. 5, pp. 787–804, May 2009.
- [33] R. Frank, S. Zadoff, and R. Heilmiller, "Phase shift pulse codes with good periodic correlation properties (corresp.)," *IEEE Trans. Inf. Theory*, vol. IT-8, no. 6, pp. 381–382, Oct. 1962.
- [34] *Technical Specification Group Radio Access Network; NR; User Equipment (UE) Radio Transmission and Reception; Part 1: Range 1 Standalone (Release 15)*, document (TS) 38.101-1, 3GPP, Version 15.3.0, 2018.
- [35] G. R. MacCartney, T. S. Rappaport, S. Sun, and S. Deng, "Indoor office wideband millimeter-wave propagation measurements and channel models at 28 and 73 GHz for ultra-dense 5G wireless networks," *IEEE Access*, vol. 3, pp. 2388–2424, 2015.
- [36] K. T. Wong, S. L. A. Chan, and R. P. Torres, "Fast-polarization-hopping transmission diversity to mitigate prolonged deep fades in indoor wireless communications," *IEEE Antennas Propag. Mag.*, vol. 48, no. 3, pp. 20–27, Jun. 2006.
- [37] T. A. Perumal, R. K. Ganti, R. D. Koilpillai, D. Jalihal, V. Ramaiyan, and K. Takei, "Channel estimation in rotating polarization based wireless communication systems," in *Proc. 22nd Nat. Conf. Commun. (NCC)*, Mar. 2016, pp. 1–6.
- [38] M. J. Feuerstein, K. L. Blackard, T. S. Rappaport, S. Y. Seidel, and H. H. Xia, "Path loss, delay spread, and outage models as functions of antenna height for microcellular system design," *IEEE Trans. Veh. Technol.*, vol. 43, no. 3, pp. 487–498, Aug. 1994.



ELIJAH I. ADEGOKE received the B.S. degree in electrical and electronics engineering from Covenant University, Nigeria, in 2009, and the M.Sc. degree in mobile communications and the Ph.D. degree in electronic engineering from Loughborough University, in 2013 and 2018, respectively. From 2010 to 2014, he worked as a Network Engineer with Telecoms Firms in Nigeria and U.K. From 2017 to 2018, he was a Research Associate with the 5G Research Centre (5GRC), Loughborough University. He is currently a Research Fellow with WMG. His work is focused on 5G channel modeling, Wi-Fi GNSS fusion/measurement, and modeling for localization in CAVs. His research interests include radio propagation and modeling, Wi-Fi positioning systems, heterogeneous wireless networks, IP mobility, self-organizing networks, Wi-Fi based V2X, and machine learning for wireless and GNSS communications.



ERIK KAMPERT received the M.Sc. and Ph.D. degrees in natural sciences from Radboud University Nijmegen, The Netherlands, in 2005 and 2012, respectively. He was with the Molecular Materials Group and the High Field Magnet Laboratory, Institute for Molecules and Materials, Radboud University Nijmegen. He continued his research as a Postdoctoral Researcher with the Dresden High Magnetic Field Laboratory, Helmholtz-Zentrum Dresden-Rossendorf, Germany, where he conducted electrical transport experiments in pulsed magnetic fields in collaboration with visiting, international scientists. In 2017, he joined the Connectivity and Communications Technology Group, WMG's Intelligent Vehicles Research Team, University of Warwick, U.K., as a Senior Research Fellow. Using his vast background in RF electromagnetics, the focuses of his current research are on 5G millimeter-wave communication for vehicular-to-everything and industrial Internet of Things applications.



MATTHEW D. HIGGINS (Senior Member, IEEE) received the M.Eng. degree in electronic and communications engineering and the Ph.D. degree in engineering from the School of Engineering, The University of Warwick, in 2005 and 2009, respectively. Remaining at The University of Warwick, he progressed through several Research Fellow positions, in association with some of the UK's leading defense and telecommunications companies. Then, he set up the Vehicular Communications Research Laboratory, which aimed to enhance the use of communications systems within the vehicular space. He is currently a Reader, leads the Connectivity and Communications Technology Research Group, WMG. He is a Senior Member of the SMIEEE, a member of the IEEE Communications Society, COMSOC, and a Fellow of the Higher Education Academy, FHEA. He is also a member of the CommNet2 Community and the EPSRC Peer Review Collage. He frequently serves as a TPC Member for key COMSOC conferences. He is a regular reviewer of leading international journals.

...